Journal of Alloys and Compounds 509 (2011) 7238–7246

Contents lists available at ScienceDirect

Journal of Alloys and Compounds

journal homepage: www.elsevier.com/locate/jallcom

Structural and elastic properties of eutectic Sn–Cu lead-free solder alloy containing small amount of Ag and In

A.A. El-Daly[a,*], Farid El-Tantawy[b], A.E. Hammad[a], M.S. Gaafar[c,1], E.H. El-Mossalamy[d], A.A. Al-Ghamdi[e]

[a] Physics Department, Faculty of Science, Zagazig University, Zagazig, Egypt
[b] Department of Physics, Faculty of Science, Suez Canal University, Ismailia, Egypt
[c] Ultrasonic Laboratory, National Institute for Standards, Tersa Street, P.O. Box 136, El-Haram, El-Giza 12211, Egypt
[d] Department of Chemistry, Faculty of Science, King Abdulaziz University, Jeddah, P.O. Box 80203, Jeddah 21569, Saudi Arabia
[e] Department of Physics, Faculty of Science, King Abdulaziz University, Jeddah, P.O. 80203, Jeddah 21569, Saudi Arabia

ARTICLE INFO

Article history:
Received 28 September 2010
Received in revised form 3 January 2011
Accepted 5 January 2011
Available online 14 January 2011

PACS:
62.20.Fe
61.82.Bg
61.66.Dk
43.35.Ae
62.20.Dc

Keywords:
Lead-free solder
Sn–Cu alloys
Microstructure
Elastic properties
Mechanical properties
Pulse-echo technique

ABSTRACT

Sn–Cu alloys have been considered as a candidate for high temperature lead-free microelectronic solders. In the present study, the change in microstructure, attenuation and elastic behavior associated with alloying of Ag and/or In into the eutectic Sn–Cu solder alloy system have been evaluated. The study involved measurements of longitudinal and shear wave velocities, attenuation, hardness, bulk and shear moduli, Young's and Poisson's ratio. The results of attenuation show that a clear attenuating effect in the ternary Sn–Cu–Ag and Sn–Cu–In alloys is realized, whereas the quaternary Sn–Cu–Ag–In solder displays an obscure attenuating effect. The obscure effect is mainly attributed to the competition for In between Sn and Ag, which results in weak interface formed between intermetallic compounds (IMCs) and β-Sn matrix. Likewise, Poisson's ratio results indicate that its value decreases with increasing the elastic moduli and ultrasonic velocities of Ag and In-containing alloys. The analyzed enhanced ductility of Sn–0.7Cu and Sn–0.7Cu–2In alloys and brittleness of Sn–0.7Cu–2Ag and Sn–0.7Cu–2Ag–2In alloys were rationalized on the basis of Poisson's ratio and the quotient of shear modulus to bulk modulus (Pugh's ratio). Microstructural analysis revealed that the origin of change in the elastic properties of the ternary and quaternary alloys is ascribed to smaller β-Sn dendrite grain dimensions and formation of new IMCs in the ternary and quaternary alloys.

1. Introduction

Following the miniaturization of contemporary solder joints, the fraction of IMCs to the total volume of solder is increasing, and hence the elastic properties of IMCs formed during soldering reaction become crucial to the reliability of solder joints [1]. For Sn-based soldering system, it has been shown that Sn–0.7Cu alloy is considered as the most promising candidate lead-free solder materials to replace eutectic Sn–Pb solder for wave, dip, and iron soldering processes. It is environmentally benign, inexpensive and has good electrical conductivity. Sn–0.7Cu solder has a melting point equal to 227 °C. Meanwhile, the primary interest is the lower cost compared with the other candidate lead-free solder alloys [2,3]. The presence of Cu in Sn-based materials leads to an improvement in resistance to thermal cycle fatigue and wetting properties due to the formation of Cu_3Sn and Cu_6Sn_5 IMCs. It also plays an important role in decreasing the rate of dissolution of Cu from the board [2,4]. However, its main disadvantage of high melting temperature, insufficient oxidation resistance characteristic and tin whiskers caused by the formation of Sn-rich phase prevents its wide practical application in microelectronic packaging industry, especially in the wave soldering applications, which are considerably forced nowadays [5–7].

Because of the technological interest, investigations of new Sn–Cu-based solder materials for electronic packaging products have never been stopped. Great achievement has been focused on developing the overall wetting and soldering properties of Sn–Cu solder and progress has been made by adding different alloying elements, such as Ag, In, Zn, and Ni [3,8–10]. The presence of the second phase has been shown to trigger the microstructural mechanism that enhances the reliability of the solder joints. Recently, Wang and Shen [9] revealed that a small amount of Ni addition to the Sn–Cu solder could effectively improve the solder properties, such as the mechanical strength and wettability. The Ni

* Corresponding author. Tel.: +20 552325030; fax: +20 552308213.
E-mail address: dreldaly99@yahoo.com (A.A. El-Daly).
[1] Current address: Physics Department, Faculty of Science, Al-Majmaah University, Al-Zulfi, Saudi Arabia.

0925-8388/$ – see front matter © 2011 Elsevier B.V. All rights reserved.
doi:10.1016/j.jallcom.2011.01.062

Table 1
Chemical composition of solder alloys (wt.%).

Alloys	Cu	Ag	In	Pb	Bi	Sb	As	Sn
Sn–0.7Cu	0.7	–	–	0.012	0.007	0.011	0.006	Bal.
Sn–0.7Cu–2.0Ag	0.7	2.0	–	0.014	0.009	0.016	0.008	Bal.
Sn–0.7Cu–2.0In	0.7	–	2.0	0.014	0.010	0.019	0.009	Bal.
Sn–0.7Cu–2.0Ag–2.0In	0.7	2.0	2.0	0.014	0.009	0.016	0.008	Bal.

particles mostly leaded to modify microstructural features and to improve the interfacial reactions between Ni and the Sn–Cu solders. Nonetheless, the improvement of mechanical properties is closely related to the amount and type of alloying elements and so, some alloying additions may not improve the properties to a desirable extent and sometimes even deteriorate them [2,10,11]. For example, Li et al. [3] found that the addition of trace P element into Sn–Cu eutectic solder led to the increase in the rate of forming void of Sn–0.7Cu solder joint. As a result, the creep fatigue of solder joint containing P such as Sn–0.7Cu–0.005P offered worse property compared to Sn–0.7Cu solder joint. Ag also plays an important role in improving the reliability of Sn–Cu solder, since it increases the creep resistance, mechanical strength and decreases the eutectic temperature of the alloys effectively [12]. However, Wu et al. [13] showed that neither the maximum ductility nor the creep resistance of the Sn–Cu-based alloy varies monotonically with the Ag content. That means, the excessive growth of IMC layer due to the high content of Ag is not predicted. Even so, the industry has to bear the fact that Sn–Ag–Cu (SAC) eutectic alloys have anisotropic properties due to the distribution of IMCs which might cause unexpected joint failures. Also, the eutectic SAC alloy can form large primary Ag_3Sn precipitates, which can deteriorate the ductility of the joints [14–16]. Therefore, identification of small microstructural changes with strong effect on the chemical and mechanical properties requires new inspection methods, which should consider additional physical variables. Pulse echo technique is an important technique for probing the elastic behavior of materials at small length scales. It is non-destructive method, inexpensive, quick, sensitive and dynamic way of measuring the modulus of elasticity. Higher precision can generally be obtained by the dynamic rather than static methods [17].

The non-destructive evaluation of the elastic properties for the solder alloys using pulse echo technique is a field of great interest. Although the elastic constants are being considered as a well known material property that builds a foundation for better understanding of various other properties such as Young's and bulk modulus, Poisson's ratio, shear modulus, hardness, attenuation coefficient and stiffness, there is still a high necessity to study in depth the effect of small amount of alloying elements such as Ag and In on the elastic properties of eutectic Sn–Cu solder alloy. Such studies could play a significant role from the standpoint of predicting the performance of the material under service conditions. The first attempt was reported lately by El-Daly and Hammad [17]. It was found that the proper additions of Cu, In and Ag into Sn–Zn eutectic solder are beneficial to encourage the formation of new IMCs. These IMCs could visibly change the elastic properties of the newly developed ternary and quaternary alloys such as the hardness, attenuation coefficient, bulk and shear moduli, Young's and Poisson's ratio. It was also found that both the hardness and reduced modulus increase as the Poisson's ratio of the alloy decreases. The aim of this work is to obtain quantitative information about the effect of Ag and/or In-additions on the longitudinal and shear ultrasonic wave velocities as well as the elastic properties and attenuation coefficient of the eutectic Sn–Cu solder alloy using pulse-echo technique. Moreover, the key factors that affect the structure and elastic constants of Sn–Cu-based solder alloys are studied and their mechanisms are also discussed. Hopefully, the results are wished useful in the further development of new solder alloys for different electronic packaging applications, such as wave soldering on single-side printed circuit boards.

2. Experimental

2.1. Materials and experimental procedure

In the present work, the lead-free Sn–0.7Cu eutectic, Sn–0.7Cu–2Ag, Sn–0.7Cu–2In, and Sn–0.7Cu–2Ag–2In solder alloys were prepared from Sn, Cu, Ag and In (purity 99.97%) as raw materials. The ingots were melted in a vacuum arc melting furnace and kept at 500 °C for 2 h. The molten solder in the crucible was chill cast in a stainless steel mold to form cylindrical ingots 10 mm in diameter and cooled down to room temperature. A cooling rate of 6–8 °C/s was achieved, so as to create the fine microstructure typically found in small solder joints in microelectronic packages [17]. Table 1 presents the chemical compositions of all studied solders. The crystal phases were analyzed by X-ray diffractometer (XRD) measured with Philips Cu-Kα radiations (λ = 1.54178 Å) in the range of 30–80 at 40 kV. The evolution of microstructure for the as-cast specimens was examined using scanning electron microscope (SEM). The solder ingots were then mechanically machined into a wire samples with a gauge length marked 2.5×10^{-2} m for each sample and 3.5×10^{-3} m in diameter. Tensile tests were carried out with a tensile testing machine (Instron 3360 Universal Testing Machine). The tests were conducted at room temperature using strain rate of 1.8×10^{-3} s^{-1} to determine the effect of Ag and In content on the mechanical properties of Sn–0.7Cu eutectic. Three specimens for each solder were tested using an Instron type machine with experimental error less than ±3%.

2.2. Pulse-echo ultrasonic testing

Ultrasonic non-destructive testing (UT) uses high frequency sound energy to conduct examinations and make measurements [18]. Ultrasonic inspection can be used for flaw detection-evaluation, dimensional measurements, material character-

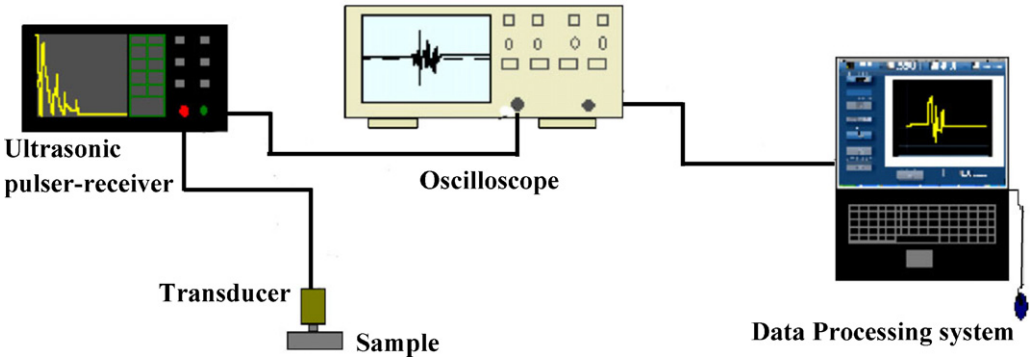

Fig. 1. Schematic representation of the ultrasonic testing (pulse-echo technique).

ization, and more. To illustrate the general inspection principle, a typical pulse-echo inspection configuration, as illustrated in Fig. 1, can be used. A standard UT inspection system consists of several functional units, such as the pulser–receiver, transducer and display devices. A pulser–receiver is an electronic device that can produce high voltage electrical pulses. Driven by the pulser, the transducer generates high frequency ultrasonic energy. The sound energy is introduced and propagates through the materials in the form of waves. When there is a discontinuity (such as a crack, precipitates or imperfections) in the wave path, part of the energy will be reflected back from the flaw surface. The reflected wave signal is transformed into an electrical signal by the transducer and is displayed on a screen. In Fig. 1, the reflected signal strength is displayed versus the time from signal generation to when an echo was received. Signal travel time can be directly related to the distance that the signal traveled. From the signal, information about the reflector location, size, orientation and other features can sometimes be gained.

In the present work, ultrasonic non-destructive technique (pulse echo technique) shown in Fig. 1 was employed to measure the mechanical wave velocity in the solder alloys. To facilitate the measurements of ultrasonic velocity, accurately, each alloy sample was first polished with 0.5 μm Al_2O_3 particles. The polished specimens are cylindrical in shape and have a length of 6 mm and a diameter of 10 mm in the gauge section. Plane parallelism between opposite faces was checked using a surface plate and its accuracy was ±25 μm. The transit time between the initiation and the receipt of the pulse appearing on the screen of a flaw detector (USIP20-Kraü tkramer) was measured using a standard electronic circuit (Hewlett Packard 54615 B). The ultrasonic wave velocity was therefore, calculated by dividing the round trip distance (twice the thickness of the sample) by the elapsed time according to the relation:

$$V = \frac{2x}{\Delta t} \tag{1}$$

where x is the sample thickness and Δt is the time interval. All velocity measurements in this study were done at 4 MHz frequency and at room temperature (25 °C). By using the Karl Deutsch transducer S12 HB4 with fundamental frequency of 4 MHz and the Kraütkramer transducer K4KY with fundamental frequency of 4 MHz, the longitudinal and shear ultrasonic wave velocities were estimated, respectively. Owing to the high accuracy of the setup, the ultrasonic wave velocity measurements with an error in the order of ±10 m/s for longitudinal velocity (V_l) and ±5 m/s for shear velocity (V_s) were determined. Uncertainty in the measurements of V_l and V_s employing t-testing has been evaluated and included in Table 2.

2.3. Density measurement

The density (ρ) of each alloy samples was measured by applying Archimedes principle at 25 °C using toluene as an immersion liquid and applying the relation:

$$\rho = \rho_b \frac{w_a}{w_a - w_b} \tag{2}$$

where ρ_b is the density of the buoyant. w_a and w_b are the sample weights in air and the buoyant, respectively. The experiment was repeated three times, and the estimated error in density measurement for all alloy samples is ±5 kg/m^3.

2.4. Determination of elastic moduli and microhardness (H)

For an isotropic solid, a number of researchers have given the empirical relationships to relate shear modulus (G), Young's modulus (E), bulk modulus (K) and Poisson's ratio (υ) for various elements. Poisson's ratio (υ) is reported to provide more information about the character of the bonding forces than any of the other elastic coefficients [19,20].

Poisson's ratio (υ) is related to E and G by:

$$\upsilon = \frac{E}{2G} - 1 \tag{3}$$

Poisson's ratio (υ) also is related to ultrasonic longitudinal wave velocity (V_l) and shear wave velocity (V_s) by:

$$\upsilon = \frac{V_l^2 - 2V_s^2}{2(V_l^2 - V_s^2)} \tag{4}$$

Additionally, V_l and V_s are related to E and G by:

$$E = \frac{3\rho V_s^2[V_l^2 - (3/4)V_s^2]}{V_l^2 - V_s^2} \tag{5}$$

$$G = \rho V_s^2 \tag{6}$$

The differential relationships of υ with (E and G) and (V_l and V_s) can be obtained by differentiating Eqs. (3) and (4), respectively. The differential forms of the above equations are:

$$\frac{d\upsilon}{\upsilon} = \frac{1}{1-(2G/E)}\left(\frac{dE}{E} - \frac{dG}{G}\right) \tag{7}$$

$$\frac{d\upsilon}{\upsilon} = \frac{2V_l^2V_s^2}{(V_l^2 - V_s^2)(V_l^2 - V_s^2)}\left(\frac{dV_l}{V_l} - \frac{dV_s}{V_s}\right) \tag{8}$$

It can be seen from Eqs. (7) and (8) that the variation in Poisson's ratio depends upon the variations in E and G and their relative values (Eq. (7)). Similarly, the relative variation in V_l and V_s also affects the variation in Poisson's ratio (Eq. (8)). It is to be noted that in any material, E and G, as well as V_l and V_s tend to vary in the same direction (increase or decrease). Hence, it is difficult to deduce from Eqs. (7) and (8) whether the variation of υ would be in the same or opposite direction to that of the elastic constants, E and G. The nature of the variation of υ would therefore depend on whether G or E is affected more by metallurgical variables. For example, if the rate of change of E (or V_l) is more than that of G (or V_s), then the right hand side of Eqs. (7) and (8) will be positive, and hence υ will vary in the same direction as that of E and G (or V_l and V_s). Similarly, if the rate of change of G (or V_s) is more than that of E (or V_l), the right hand side of Eqs. (7) and (8) will be negative, and hence υ will vary opposite to E and G (or V_l and V_s). From the first law of thermodynamics, it can be seen that E, K and G are positive, and seeing as $K = E/3(1-2\upsilon)$ and $G = E/2(1+\upsilon)$. However, for isotropic solids, υ is bounded practically by 0 and 1/2. For $\upsilon = 1/2$, no volume change occurs during deformation [17]. The microhardness H was calculated from Young's modulus E and Poisson's ratio υ according to the relationship [21]:

$$H = \frac{E(1-2\upsilon)}{6(1+\upsilon)} \tag{9}$$

Conversely, the attenuation effect and elastic behavior are ultrasonic property. Ultrasonic spectral analysis involves characterization of the waveform after the wave has propagated through a material. This method has been investigated in the last decades in order to explore microstructural changes in the studied materials by evaluating frequency and amplitude of acoustic signals. Longitudinal wave velocity and the attenuation coefficient were obtained from the amplitude and position quantification of the back-wall echo and its first two multiples. Attenuation coefficients α were calculated from the echo height ratio of the consecutive peaks according to the relationship [22]:

$$\alpha\,(\mathrm{dB/mm}) = 20\log\frac{A_i/A_j}{2x} \tag{10}$$

where A_i and A_j are the echo heights of consecutive peaks i and j, respectively, and x is the specimen thickness in mm.

3. Results and discussion

3.1. Microstructure change with addition of Ag and In

In order to develop a new Sn–0.7Cu-based lead-free solder with better properties, small amounts of Ag and In were selected as an alloying additions, which have a little solubility in β-Sn near room temperature, high oxidation resistance and which were expected to be fine nuclei for solidification [6,19]. Fig. 2a–d shows some morphological changes resulting from Ag and In additions into Sn–Cu eutectic solder, where β-Sn dendrite formation in the eutectic regions are observed. The microstructure of as-solidified Sn–0.7Cu solder alloy exhibits a typical rapidly solidified Sn–Cu eutectic microstructure (see Fig. 2a). It consists of the light-gray coarse β-Sn phase (with a size of 10–40 μm) surrounded by dark eutectic

Table 2
Ultrasonic wave velocities (longitudinal V_l and shear V_s) and density (ρ) values for the given solder alloys.

Alloy	V_l (m/s)	V_s (m/s)	ρ (kg/m^3)	Error %		
				V_l	V_s	ρ
Sn–0.7Cu	3272	1863	7384	0.83	0.72	0.64
Sn–0.7Cu–2.0Ag	3349	1960	7280	0.69	0.95	0.82
Sn–0.7Cu–2.0In	3312	1892	7219	0.92	0.64	0.53
Sn–0.7Cu–2.0Ag–2.0In	3379	1954	7297	0.54	0.48	0.37

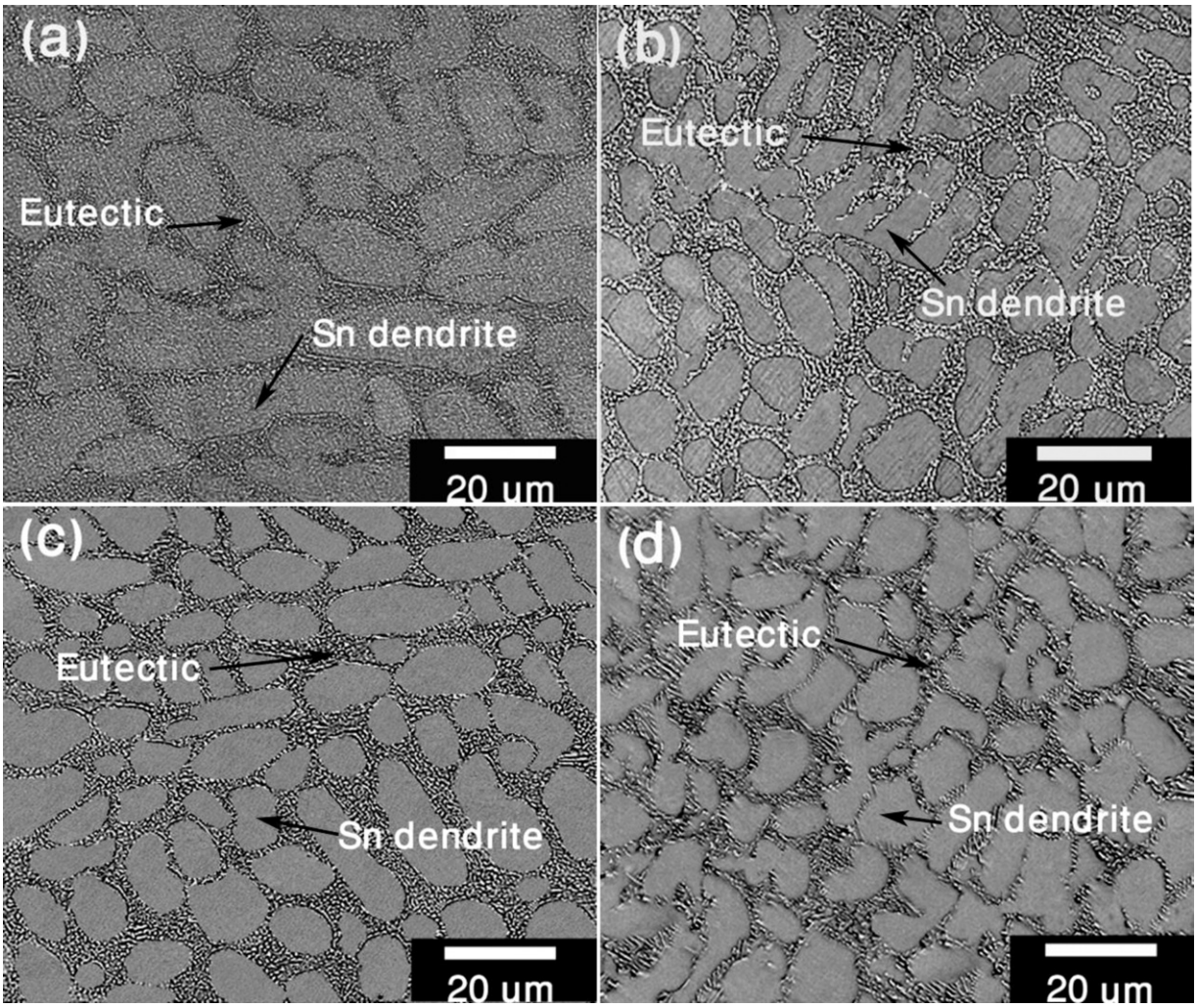

Fig. 2. Microstructure of as-cast solder alloys: (a) Sn–0.7Cu, (b) Sn–0.7Cu–2Ag and (c) Sn–0.7Cu–2In and (d) Sn–0.7Cu–2Ag–2In.

networks of β-Sn and Cu_6Sn_5 IMCs (fine particles with a size of (~1 μm)). The finer particles were identified as being Cu_6Sn_5 IMCs according to the XRD analysis (Fig. 3a). The morphology of the eutectic region is superfine and there are no big block-like Cu_6Sn_5 particles in the structure. This effect could be attributed to the fast cooling rate employed during the production of these alloys.

With the addition of Ag and/or In into the Sn–0.7Cu solder alloy, all the new alloys exhibit mainly a binary-phase structure of Cu_6Sn_5 IMCs and a β-Sn dendritic phase. Moreover, the β-Sn dendrites were refined to some extents. It also provides a fine and uniform distribution of new IMCs in the eutectic regions of the solidified microstructure. Since the morphology of IMCs depends on the fast cooling rate in the present study, it is difficult to distinguish the shape difference between all the IMCs found in the Sn–0.7Cu-based alloys as shown in Fig. 2a–d, which are consistent with the testing results given Sun et al. [23]. They reported that the slow cooling rate could effectively deteriorate the solder properties such as reducing the solder joint's ductility, inducing brittle fracture, influencing crack initiation and accelerating the fatigue crack growth kinetics due to the formation of large IMCs.

However, in case of Sn–0.7Cu–2Ag ternary system (Fig. 2b), the microstructure of lead-free Sn–0.7Cu–2Ag solder was composed of small β-Sn dendrites (5–25 μm), Ag_3Sn and Cu_6Sn_5 IMCs as was confirmed by XRD analysis (Fig. 3b), which appeared similar to those reported in the same crystal family of the SAC solder alloys [6,19]. The formations of such small β-Sn dendrites and new IMCs particles have been recognized to reinforce the solder matrix and to improve the mechanical properties of the solder alloy [23]. Similar variation features also appeared for the Sn–0.7Cu–2In alloy (Fig. 2c), where the eutectic regions were identified by means of XRD to be Sn, Cu_6Sn_5 and γ-In Sn_4 IMCs (Fig. 3c).

Compared to the separate addition of Ag and In, the dual addition of Ag and In create supplementary modification in the microstructure of the Sn–0.7Cu solder. The large β-Sn dendrites also are refined to 5–20 μm and decorated by the Sn, Cu_6Sn_5, Ag_3Sn, γ-$InSn_4$ and In_4Ag_9 IMCs in the eutectic regions as shown in Figs. 2(d) and 3(d). Although the combined effects of such structures are somewhat complicated, it is remarkable to note that In has a greater affinity to reduce the activity of Ag by forming Ag–In IMCs, leading to rapid decrease in the driving force of Ag_3Sn IMCs formation. Such microstructure could impair the mechanical properties of the quaternary Sn–0.7Cu–2Ag–2In alloy to some extents. This can be ascribed to the competition for In between Sn and Ag, which results in weak interface formed between the new IMCs and β-Sn matrix. Thus, the formation of Ag–In IMCs phase cannot favor the activation property of the alloy. El-Daly and Hammad studied the effect of dual addition of Ag and Cu on solidification kinetic and microstructure development of eutectic Sn–Zn and observed a similar phenomenon [15]. Additionally, this is similar to the observation with indium addition to SnAgCu solder made by

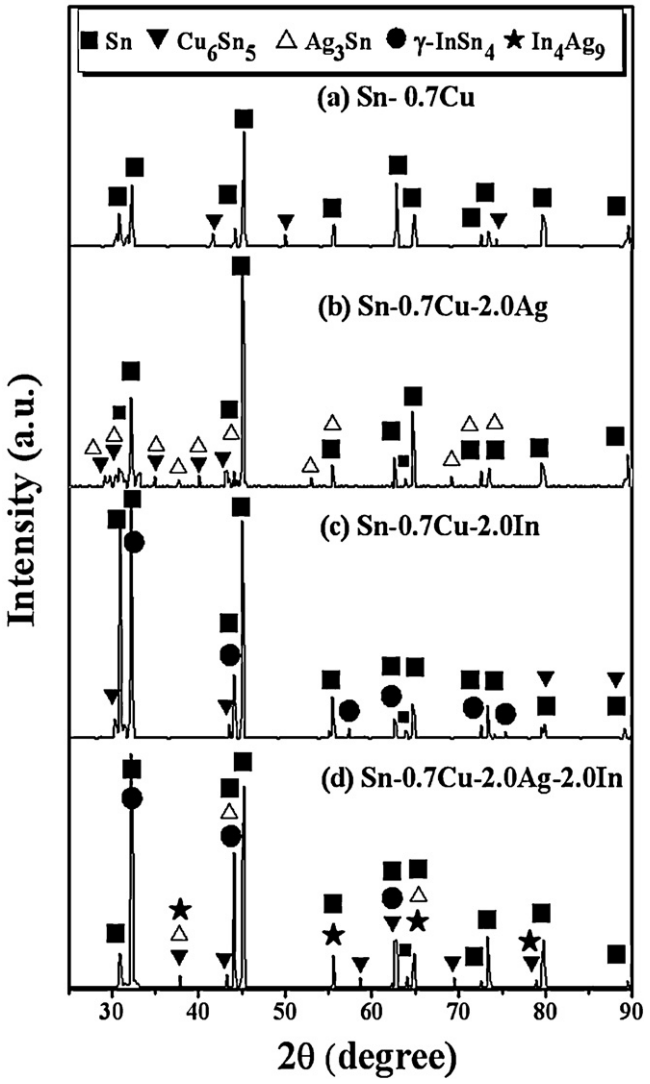

Fig. 3. XRD patterns of as-cast solder alloys: (a) Sn–0.7Cu, (b) Sn–0.7Cu–2.0Ag, (c) Sn–0.7Cu–2.0In and (d) Sn–0.7Cu–2.0Ag–2.0In.

Gao et al. [19]. It was established by Gao et al., that the appearance of the Ag_3Sn compounds is changed. About 56% of Sn is replaced by indium to form $Ag_3(In_{0.56}Sn_{0.44})$. Also, the large Ag–In–Sn IMCs were appeared in a spherical form. So, it may be stated that the interfacial energy per unit area between Ag–In–Sn IMCs and molten In-containing solder is higher than that between Ag_3Sn and molten SnAgCu. For this reason, the morphology of Ag–In–Sn IMC in the solder matrix becomes spherical to possess less free energy thermodynamically.

3.2. Effect of alloy composition on the ultrasonic wave velocities and density (ρ)

A comparison of the longitudinal, transverse ultrasonic velocities and density values obtained for all Sn–0.7Cu-based solders is shown in Fig. 4 and Table 2. It can be seen that all the velocities increased and the density decreased with the additions of Ag, and In elements. The reason for these velocity differences comes from the fact that the wave signal is sensitive to different changes in material state associated with the formation of new IMCs precipitates and its structural evolution. In other words, the difference between the elasticity moduli of the matrix and IMCs can affect the stressed state of the material. Hence, it would be expected that the

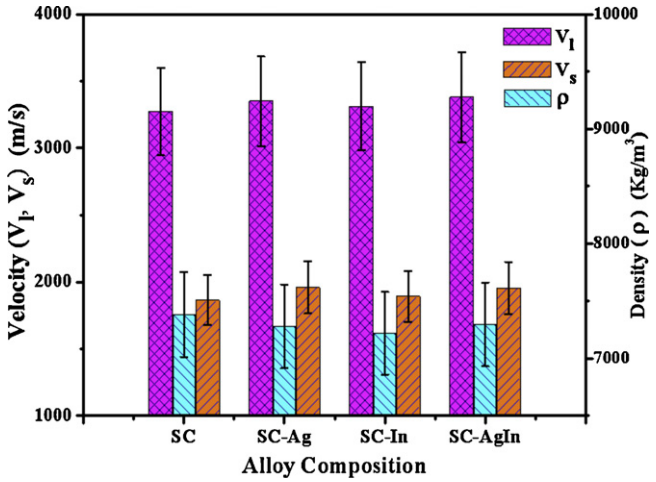

Fig. 4. Ultrasonic wave velocities (longitudinal V_l and shear V_s) and density (ρ) values for Sn–0.7Cu (SC), Sn–0.7Cu–2.0Ag (SC–Ag), Sn–0.7Cu–2.0In (SC–In) and Sn–0.7Cu–2.0Ag–2.0In (SC–AgIn) alloys.

presence of new IMCs precipitate should considerably modify the ultrasonic wave velocity [17]. This statement is consistent with that reported by other researchers [22]. They reported that the velocity of an ultrasonic wave V can be represented as a function of the volumetric fractions of all present phases as:

$$V = \sum f_i V_i \tag{11}$$

where f_i is the volumetric fraction of each existing phase and V_i is the wave velocity in each phase in the material. Due to the extremely high volumetric fraction of new IMCs, which precipitate locally at the eutectic regions, the applicability of any velocity measurement techniques could be expected. In the meantime, the separate addition of Ag can result in higher velocity than In-addition due to the formation of hard Ag_3Sn IMC. This hypothesis is consistent with the result of quaternary Sn–0.7Cu–2Ag–2In solder, as the dual addition of Ag and In lead to a slight variation of velocity values compared with the separate addition of Ag into the Sn–0.7Cu solder.

From the fundamental point of view our results appear interesting as well: firstly, the shear wave velocities are less than (about half of that of) longitudinal wave velocities. Thus, the transit time of shear wave is more than (about double of) that of longitudinal wave velocity for the same thickness of the specimen. As the shear wave velocity is affected more than the longitudinal wave velocity due to any microstructural variation and also the error in its measurement is less, it can be concluded that ultrasonic shear wave velocity is a better parameter for microstructural characterization as compared to longitudinal wave velocity, which is in good agreement with the literature data [17,25]. This illustrates that our method for calculating the elastic properties is reasonable and reliable.

Secondly, the Poisson's ratio υ value will vary on the contrary to V_l and V_s (or E and G), since the rate of change of V_s is greater than that of V_l as seen in Tables 2 and 4. This can be explained by the fact that the calculation of both the Poisson's ratio υ and velocities (or E and G) depends on the contact areas through Eqs. (7) and (8). Previous studies also have indicated that such behavior was obtained for various solid isotropic materials [17,25]. Conversely, the observed change of ρ values could be explained by the change in the volume fraction of the newly developed IMCs in the ternary and quaternary solder alloys as well as their axial ratio and densities [17].

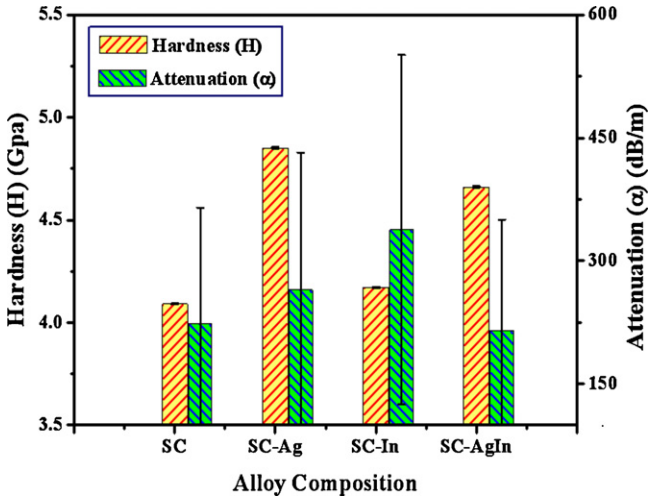

Fig. 5. Hardness (H) and attenuation coefficient (α) values for Sn–0.7Cu (SC), Sn–0.7Cu–2.0Ag (SC–Ag), Sn–0.7Cu–2.0In (SC–In) and Sn–0.7Cu–2.0Ag–2.0In (SC–AgIn) alloys.

3.3. Effect of alloy composition on the attenuation coefficient (α) and hardness (H)

Attenuation α is widely used as an ultrasonic parameter. It represents a relative energy loss experienced by an ultrasonic plane wave per unit length of a solid sample [17]. Identification of small microstructural changes with strong effect on the chemical and mechanical properties requires inspection by measurements of attenuation and hardness.

Fig. 5 and Table 3 show some aspects regarding the attenuation values in the tested solders. It should be noted, by a simple comparison of the attenuation coefficients, that the differentiation between the alloying effects is reasonable. Separate addition of Ag and In into the Sn–0.7Cu eutectic solder increase the α value from 224 ± 55 to 265 ± 94 and 338 ± 42 dB/m, respectively. In contrast, the dual addition of Ag and In decreases it to 215 ± 62 dB/m. The observed change of attenuation could be explained by the microstructural changes of the studied solders as follows; the increase in α value of the ternary alloys could be related to the formation of new Ag_3Sn and γ-$InSn_4$ IMCs as well as the decrease in size of its β-Sn dendrites. Because of the high difference in acoustic properties between the β-Sn dendrites and the new Ag_3Sn and γ-$InSn_4$ IMCs, an additional reduction in the wave intensity is expected. Thus, the formation of new Ag_3Sn and γ-$InSn_4$ IMCs can justify a detectable increase of the attenuation values in the ternary solders.

Generally, problems resulting from the evaluation of microstructural changes using a unique ultrasonic parameter not only originate from the large dimensional difference between the ultrasonic wavelength and the microstructural component size of the alloy, but also by the multiple modifications that take place in the type and volume fraction of these components [22,24]. Thus, it would be expected that the dual addition of Ag and In should considerably modify attenuation coefficient of the binary eutectic solder. The observed decrease in α value of Sn–0.7Cu–2Ag–2In solder could be related to the formation of new Ag_3Sn, In_4Ag_9 and γ-$InSn_4$ IMCs in the eutectic region. Since Ag and In have a stronger affinity than Ag and Sn and thus the interaction between Sn and Ag would be seriously weakened due to the existence of In. As a result, the higher affinity of In to reduce the activity of Ag by forming In_4Ag_9 IMCs can justify a rapid decrease of the driving force of Ag_3Sn and γ-$InSn_4$ IMCs formation. Hence, the moderate or high modifications in these IMCs can rationalize the attenuation values. Accordingly, the attenuation decrease in Sn–0.7Cu–2Ag–2In specimens mainly could arise due to an extensive In_4Ag_9 IMC precipitation in the eutectic region and it is not originated from the scattering attenuation caused by Ag_3Sn and γ-$InSn_4$ IMCs as seen before.

Table 3
Hardness (H) and attenuation coefficient (α) values for the given solder alloys.

Alloys	H (GPa)	α (dB/m)	Errors (%)	
			H	α
Sn–0.7Cu	4.09	224	±1.22	±24.5
Sn–0.7Cu–2.0Ag	4.85	265	±0.62	±35.4
Sn–0.7Cu–2.0In	4.17	338	±0.85	±7.1
Sn–0.7Cu–2.0Ag–2.0In	4.66	215	±1.13	±28.8
Cu_6Sn_5	6.12	–	±0.17	–
[26]	3.6	–	−5.9	–
	6.1	–	±0.53	–
	6.5	–	±0.30	–
Ag_3Sn	3.25	–	±0.18	–
[26]	2.37	–	±3.13	–
	2.9	–	±0.20	–
Pure Sn [26]	0.14	–	±0.02	–

The influence of Ag and In-additions reinforcement on the hardness (H) value is also summarized in Fig. 5 and compared with literature values obtained through nanoindentation [26] in Table 3. By considering the variations observed in H value as a function of Ag and In-additions, we note that the formation of new IMC particles is directly responsible for the higher hardness values observed in these materials in agreement with Dudek and Chawla [26]. They reported that all IMCs had maximum loads higher than that of pure Sn as seen in Table 3. However, Table 3 also shows that the binary Sn–0.7Cu eutectic solder had the lowest average hardness value of 4.09 ± 0.05 GPa. Because of the strengthening effect of Ag_3Sn phase, the evaluated hardness of Sn–0.7Cu–2Ag solder (4.85 ± 0.03 GPa) is the highest among the four solder alloys. It appears that the presence of Ag_3Sn in Sn–0.7Cu–2Ag solder might acts as potential sites for obstructing localized elastic deformation of the matrix during the motion of linear dislocations and grain boundaries. Alternatively, the decrease in H value from Sn–0.7Cu–2Ag to Sn–0.7Cu–2Ag–2In solder would then be related to the partially conversion from Ag_3Sn to In_4Ag_9 as deduced from XRD (Fig. 3). However, a higher H value often suggests a bigger change in the effective acting stress of IMCs precipitates, which reflects as an increase of the atomic bonding forces between the constituents of IMCs [17]. This is similar to the observation with In addition to Sn–3.5Ag made by [14]. It was found that the decrease in hardness value resulted in higher bonding force between Ag and Sn than that of In with Ag or Sn.

3.4. Effect of alloy composition on elastic moduli and Poisson's ratio

Elastic moduli and Poisson's ratio υ are apparently important parameters as a chain to understand the correlation between the structural characteristics and relevant mechanical properties. The first one gives a global and often macroscopic view of a material stiffness. It reflects both the inter-atomic bonding energies and the connectivity [27]. The second, the Poisson's ratio provides more information about the characteristics of the bonding forces than any of the other elastic constants. It has a value of between 0 and +0.5 depending on the compressibility of a material. So, the larger the υ is, the more ductile the alloy becomes [17]. It is also quantifying the material's resistance to dilatation and shearing. Fig. 6 and Table 4 present the typical dynamic moduli and Poisson's ratio measured by the pulse echo technique for the Sn–0.7Cu-based solders at room temperature, which show the pure elastic materials' response. It can be seen that the Sn–0.7Cu–2Ag solder alloy had the highest Young's modulus (69.3 GPa) and reduced Poisson's ratio (0.24) in comparison to all the Sn–0.7Cu-based solders. On the other hand,

Table 4
Experimental values of shear modulus (G), bulk modulus (K), Young's modulus (E), Poisson's ratio (υ) and(G/K) ratio.

Alloy	G (GPa)	K (GPa)	E (GPa)	υ	G/K	Errors %			
						G	K	E	υ
Sn–0.7Cu	25.62	44.86	64.6	0.26	0.571	3.2	0.47	1.08	0.56
Sn–0.7Cu–2.0Ag	27.95	44.42	69.3	0.24	0.629	2.4	0.43	0.96	3.9
Sn–0.7Cu–2.0In	25.85	44.76	65	0.258	0.578	0.6	0.5	1.03	3.02
Sn–0.7Cu–2.0Ag–2.0In	27.85	46.21	69.6	0.249	0.603	0.2	0.15	0.67	3.53

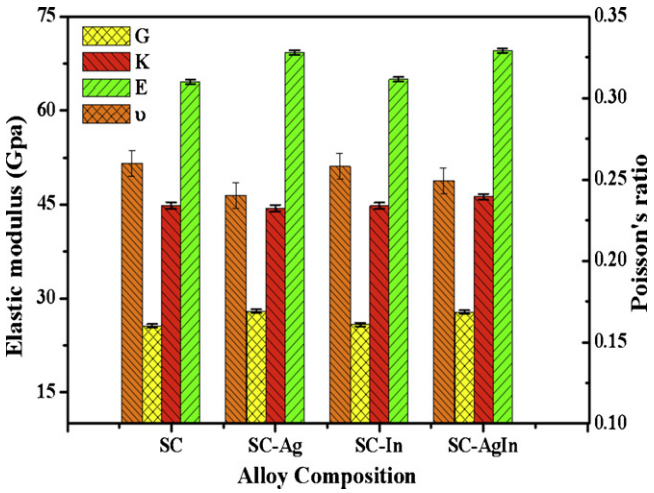

Fig. 6. Elastic moduli: shear modulus (G), bulk modulus (K), Young's modulus (E) and Poisson's ratio (υ) for Sn–0.7Cu (SC), Sn–0.7Cu–2.0Ag (SC–Ag), Sn–0.7Cu–2.0In (SC–In) and Sn–0.7Cu–2.0Ag–2.0In (SC–AgIn) alloys.

the Sn–0.7Cu–2In solder has the lowest Young's modulus value of 65.0 GPa, which is slightly higher than that of binary Sn–0.7Cu solder (64.6 GPa). It is important to recognize that In–Sn IMC is the softest phase, whereas the hardest phase is the Ag–Sn IMC since it possesses a higher hardness and elastic moduli. However, according to our results in Table 4, the elastic constants decreased with increasing Poisson's ratio, and it was minimum when Poisson's ratio was maximum and vice versa [25]. Similar observations were also obtained in the literature data [17,25]. In addition, the bulk modulus of Sn–0.7Cu–2Ag (44.42 GPa) is much smaller than that of the four solder alloys, and it implies that Sn–0.7Cu–2Ag solder has the highest compressibility.

Similar variation tendency of Poisson's ratio and ductility upon the change of alloying composition was observed, which shows the maximum peak around the same composition of Sn–0.7Cu solder (see Figs. 6 and 8). The sample with the largest ductility of 39.1% has the largest Poisson's ratio value of 0.26 among the other solders. The driving force for microstructural change has been established as the Poisson's ratio and ductility values shrink with the formation of new IMCs in the ternary and quaternary alloys (see Tables 4 and 5). The phenomenon may be due to the intrinsic structural characteristics of IMCs consisting of packed atomic. This kind of microstructure allows efficient packing of atom clusters in fixed compositions that show markedly different properties [17].

The large Poisson's ratio obtained for the studied samples may be directly connected to amount of valence electrons. Since the value of υ for covalent materials is small ($\upsilon = 0.1$), whereas for ionic materials a typical value of υ is 0.25 [17]. In our case the value of Poisson's ratio υ vary from 0.24 (Sn–0.7Cu–2Ag alloy) to 0.26 (Sn–0.7Cu alloy). This implies that the Poisson's ratios serve to describe the redistribution of the electrons along with the bonding process, showing that there is an ionic contribution in the interatomic bonding for these alloys should be assumed.

As the elasticity of materials cannot be evaluated by elastic moduli alone, another important factor is the quotient of shear modulus to bulk modulus (G/K) can be taken as a measure of elasticity as proposed by Pugh [28]. The shear modulus G represents the resistance to plastic deformation, while the bulk modulus K represents their resistance to fracture [4]. According to the Pugh and Zhou's discussion [28,29], the Pugh's ratio (G/K) can empirically links the plastic property of metals and IMCs to the G and K values. If $G/K < 0.57$, the material behaves in a ductile manner, otherwise the material behaves in a brittle manner. Table 4 presents the Pugh's ratios of the four systems. Pugh's ratios are 0.5711, 0.6292, 0.5775 and 0.6027 for Sn–0.7Cu eutectic, Sn–0.7Cu–2Ag, Sn–0.7Cu–2In, and Sn–0.7Cu–2Ag–2In solder alloys, respectively, which are slightly increased by about 10, 1.3 and 5.5% due to the addition of Ag and/or In into the eutectic Sn–0.7Cu alloy. These results suggest a slight decrease of room temperature ductility for Sn–0.7Cu-based alloys. However, Sn–0.7Cu and Sn–0.7Cu–2In have similar values for Pugh's ratio, which indicate that In is benefited to improve the strength of eutectic Sn–0.7Cu alloy without losing its ductility. Although the above evaluation method is highly simplistic, it nevertheless indicates the tendency of ductility and brittleness of the four solder alloys.

3.5. Alloying effect on mechanical performance

A stress–strain attitude was employed to investigate the mechanical properties of the four solder alloys in this study. Fig. 7

Table 5
Tensile properties of the solders Sn–0.7Cu, Sn–0.7Cu–2.0Ag, Sn–0.7Cu–2.0In and Sn–0.7Cu–2.0Ag–2.0In solder alloys at $T = 25\,^{\circ}C$ and $\dot{\varepsilon} = 1.8 \times 10^{-3}\,s^{-1}$.

Alloy	UTS (MPa)	YS (MPa)	EL (%)	E (GPa)	Errors %			
					UTS	YS	EL	E
Sn–0.7Cu	22	16.3	39.1	42.5	±1.3	±3.3	±2.3	±0.35
Sn–0.7Cu–2.0Ag	31.5	26.8	33.4	64.6	±2.6	±2.7	±2.8	±0.57
Sn–0.7Cu–2.0In	30	23.5	34.1	45.5	±2.2	±1.9	±3.1	±0.19
Sn–0.7Cu–2.0Ag–2.0In	34.6	30	18.2	65.3	±1.8	±2.5	±2.9	±1.02
Sn–0.7Cu [2]	20	17	33.6	–	±1.0	±1.0	±3.0	–
Sn–0.7Cu [2]	22	15	39	–	–	–	–	–
Sn–37Pb [2]	31	27	48	–	–	–	–	–
Sn/3.5 wt.% Ag [2]	26.7	22.5	24	–	–	–	–	–
SAC105 [30]	28.64	22.56	40	44.18	3.4	−4.3	±1.0	−3.6
SAC205 [30]	35.78	28.95	39	48.43	4.2	2.1	±1.5	−4.4
SAC305 [30]	39.54	31.86	40	54.47	−1.6	−4.2	±1.5	−4.2

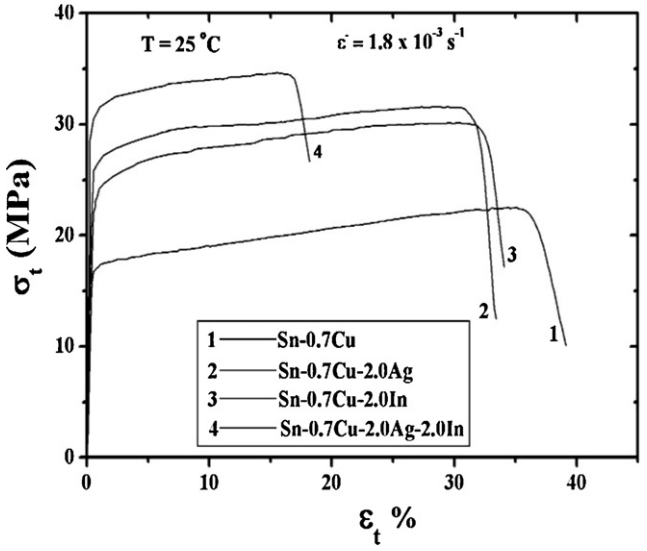

Fig. 7. Comparative tensile stress–strain curves obtained at $T = 25\,^{\circ}C$ and $\dot{\varepsilon} = 1.8 \times 10^{-3}\ s^{-1}$ for: (1) Sn–0.7Cu, (2) Sn–0.7Cu–2.0Ag, (3) Sn–0.7Cu–2.0In and (4) Sn–0.7Cu–2.0Ag–2.0In alloys.

shows the typical tensile stress–strain curves of the lead-free solder specimens at room temperature and constant strain rate of $1.8 \times 10^{-3}\ s^{-1}$. The average values of ultimate tensile strength (UTS), yield stress (YS), elongation (EL) and Young modulus (E) of the solder alloys are summarized in Fig. 8 and compared in Table 5 with data from literature on SAC alloys [2,30]. Fig. 7 illustrates that strain hardening instead of strain softening has occurred for all specimens, which can be ascribed to the strengthening mechanism of the IMCs in the alloy matrix. The newly developed IMCs in the alloy matrix are effective in increasing the dislocation density and obstacles that restrict the motion of dislocation, which is a lucid demonstration of pinning grain boundaries of β-Sn dendrites. From Table 5, the UTS values of the as-solidified Sn–0.7Cu eutectic, Sn–0.7Cu–2Ag, Sn–0.7Cu–2In and Sn–0.7Cu–2Ag–2In alloys were 22.0, 31.5, 30.0 and 34.6 MPa, respectively. The elongations to failure for the four solder alloys, respectively, were 39.2, 33.4, 34.1and 18.2%. The results revealed that the dual addition of Ag and In displayed the highest UTS and lowest ductility of the four solders investigated whereas, the separate addition of Ag and In revealed significant improvement in the UTS with appropriate ductility. By comparing the studied alloys with the reported values for Sn–0.7Cu and SAC alloys [2,30], it is noted that the UTS, YS, E and ductility values attained for Sn–0.7Cu and Sn–0.7Cu–2Ag alloys are consistent with that of Sn–0.7Cu and SAC alloy values (Table 5). The increase in YS and UTS can be analyzed in terms of morphological characteristics associated with grains and secondary phases. Che et al. [30] showed that the Ag content can increase the amount of Ag_3Sn and Cu_6Sn_5 IMC precipitates and refine the β-Sn dendrites in Sn–Ag–Cu solder, which makes the solder exhibit high strength. However, in this study, grain size refinement also plays a role to increase the material's strength. This strengthening effect is significant as the variations in grain size and secondary phases are substantial with the addition of Ag and In elements (see Figs. 2 and 3).

The E-modulus, defined as the slope of the linear part in the stress–strain relationship, was also analyzed. When measuring the E-modulus it is important to be aware that solders have both elastic and plastic response at the instant of load application [7]. Hence, the E values are described as the static modulus, which is generally referred as the apparent or effective elastic modulus since the behavior is obviously not purely elastic [17]. The comparison of static modulus values (Table 5) with dynamic modulus measured

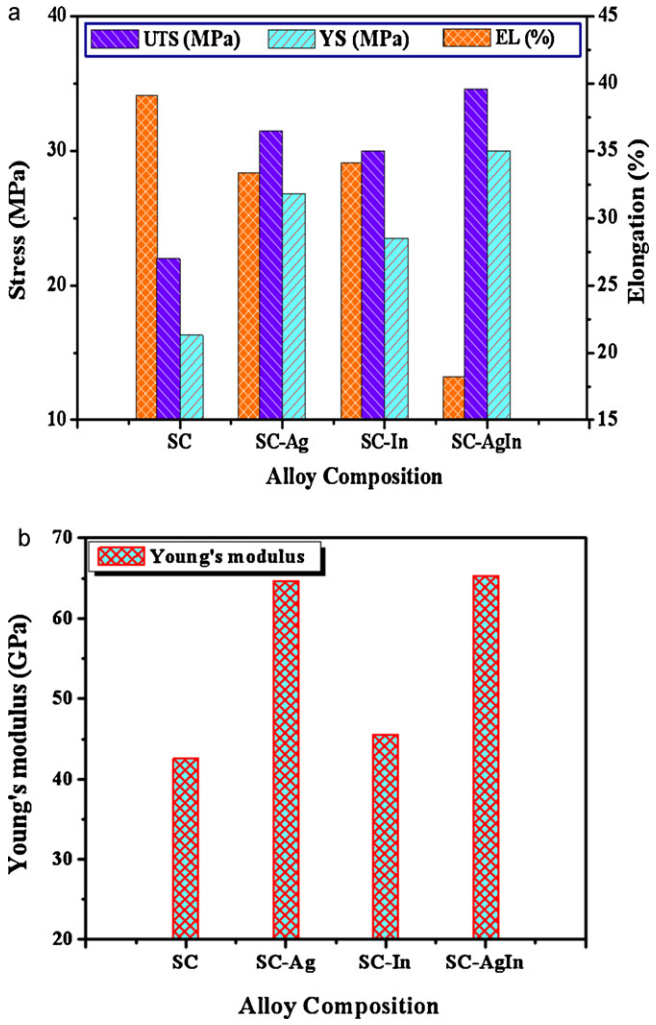

Fig. 8. Mechanical properties of the samples: (a) ultimate tensile strength (UTS), yield stress (YS), elongation and (b) Young's modulus (E).

by the ultrasonic wave method (Table 4) indicates that the dynamic Young's modulus values are larger than that of the static modulus. This means that the static modulus usually includes small inelastic deformations or time-dependent deformations such as creep, whereas, dynamic modulus measured by the ultrasonic wave method typically eliminates the inelastic deformation due to rapid wave propagation. Thus, it is of value to suggest that the dynamic modulus measured by the pulse echo technique is more accurate than the static modulus measured from the slope of the linear part in the stress–strain relationship. A similar trend has been reported by [7,17], which showing an obvious effects of inelastic deformations on the E-modulus.

4. Conclusions

In summary, we have investigated the structural and elastic properties of Sn–0.7Cu-based solders containing small amount of Ag and In elements. We calculated the sound velocities and densities for the investigated alloys. We derived the hardness, the attenuation coefficient, the bulk and shear moduli, Young's and Poisson's ratio for Sn–0.7Cu eutectic, Sn–0.7Cu–2Ag, Sn–0.7Cu–2In and Sn–0.7Cu–2Ag–2In solders. The results are summarized as follows:

1. From microstructure examination, some new phases are developed compared to Sn–0.7Cu eutectic solder alloy such as Ag_3Sn for Sn–0.7Cu–2Ag solder, γ-$InSn_4$ for Sn–0.7Cu–2In solder, γ-$InSn_4$ and In_4Ag_9 for Sn–0.7Cu–2Ag–2In solder, along with the peaks of β-Sn phase and Cu_6Sn_5 phase in all alloys.
2. According to the results above, an important finding is that the elastic modulus can be correlated with the formation of new intermetallic phases. The Sn–0.7Cu–2Ag lead-free solder proved to be promising in that it gave good combination of higher UTS and appropriate ductility than the other three alloys, which was possible due to the formation of hard Ag_3Sn precipitates.
3. Both the hardness and reduced modulus increase as the Poisson's ratio of the alloy decreases.
4. By analyzing Pugh's ratio, it was found that the additions of Ag and/or In can reduce the room temperature ductility of Sn–0.7Cu eutectic to some extent.
5. The value of Poisson's ratio υ varies from 0.24 for Sn–0.7Cu–2Ag to 0.26 for Sn–0.7Cu eutectic. This implies that a higher ionic contribution in inter-atomic bonding of all alloys should be assumed.
6. The solving for most manufacturing problems may be occurred by appropriate choice of components with α and υ control strategy.

References

[1] J. Chen, Y. Lai, Microelectron. Reliab. 49 (2009) 264–268.
[2] M.E. Alam, S.M.L. Nai, M. Gupta, J. Alloys Compd. 476 (2009) 199–206.
[3] G. Li, Y. Shi, H. Hao, Z. Xia, Y. Lei, F. Guo, J. Alloys Compd. 491 (2010) 382–385.
[4] F.Y. Hung, T.S. Lui, L.-H. Chen, N.T. He, J. Alloys Compd. 457 (2008) 171–176.
[5] S. Lin, C. Yang, S. Wu, S. Chen, J. Electron. Mater. 37 (2008) 498–506.
[6] Y.Y. Lee, H.W. Tseng, Y.H. Hsiao, C.Y. Liu, JOM 61 (6) (2009) 51–58.
[7] C. Andersson, P. Sun, J. Liu, J. Alloys Compd. 457 (2008) 97–105.
[8] L. Lin, J. Song, Y. Lai, Y. Chiu, N. Lee, J. Uan, Microelectron. Reliab. 49 (2009) 235–241.
[9] C.H. Wang, H.T. Shen, Intermetallics 18 (2010) 616–622.
[10] H. Nishikawa, J.Y. Piao, T. Takemoto, J. Electron. Mater. 35 (2006) 1127–1132.
[11] Y. Sun, J. Liang, Z. Xu, G. Wang, X. Li, J. Mater. Sci.: Mater. Electron. 19 (2008) 514–521.
[12] Y. Yu, Z. Xia, F. Guo, Y. Shi, J. Electron. Mater. 37 (2008) 975–981.
[13] C.M.L. Wu, D.Q. Yu, C.M.T. Law, L. Wang, J. Electron. Mater. 31 (2002) 928–932.
[14] S.E. Negm, H. Mady, A.A. Bahgat, J. Alloys Compd. 503 (2010) 65–70.
[15] A.A. El-Daly, A.E. Hammad, Mater. Sci. Eng. A 527 (2010) 5212–5219.
[16] H.J. Lin, T.H. Chuang, J. Alloys Compd. 500 (2010) 167–174.
[17] A.A. El-Daly, A.E. Hammad, J. Alloys Compd. 505 (2010) 793–800.
[18] E.P Papadakis, T.P. Lerch, in: M. Levy, H.E. Bass, R.R. Stern (Eds.), Handbook of Elastic Properties of Solids, Liquids and Gases, vols. I–IV, Academic Press, 2001.
[19] L. Gao, S. Xue, L. Zhang, Z. Sheng, F. Ji, W.S. Dai, L. Yu, G. Zeng, Microelectron. Eng. (2010), doi:10.1016/j.mee.2010.04.007.
[20] S.K. Seo, S.K. Kang, D.Y. Shih, H.M. Lee, Microelectron. Reliab. 49 (2009) 288–295.
[21] M.A. Sidkey, M.S. Gaafar, Physica B 348 (2004) 46–55.
[22] J. Stella, J. Cerezo, E. Rodríguez, NDT&E Int. 42 (2009) 267–274.
[23] P. Sun, C. Andersson, X. Wei, Z. Cheng, D. Shangguan, J. Liu, Mater. Sci. Eng. B 135 (2006) 134–140.
[24] R.M. Shalaby, Cryst. Res. Technol. 45 (2010) 427–432.
[25] A. Kumar, T. Jayakumar, B. Raj, K.K. Ray, Acta Mater. 51 (2003) 2417–2426.
[26] M.A. Dudek, N. Chawla, Intermetallics 18 (2010) 1016–1020.
[27] H. Fua, W. Peng, T. Gao, Mater. Chem. Phys. 115 (2009) 789–794.
[28] S.F. Pugh, Philos. Mag. 45 (1954) 823–843.
[29] W. Zhou, L. Liu, B. Li, P. Wua, Q. Song, Comput. Mater. Sci. 46 (2009) 921–931.
[30] F.X. Che, W.H. Zhu, E.S.W. Poh, X.W. Zhang, X.R. Zhang, J. Alloys Compd. 507 (2010) 215–224.